Optics & Laser Technology 139 (2021) 106977

Contents lists available at ScienceDirect

Optics and Laser Technology

journal homepage: www.elsevier.com/locate/optlastec

Full length article

Optical fiber interferometer for temperature-independent refractive index measuring over a broad range

J.A. Flores-Bravo [a], M.A. Illarramendi [b], Joseba Zubia [a], Joel Villatoro [a,c,*]

[a] Department of Communications Engineering, University of the Basque Country UPV/EHU, Bilbao 48013, Spain
[b] Department of Applied Physics I, University of the Basque Country UPV/EHU, Bilbao 48013, Spain
[c] IKERBASQUE, Basque Foundation for Science, Bilbao 48013, Spain

ARTICLE INFO

Keywords:
Optical fiber sensors
Fabry-Perot interferometers
Refractometers
Refractive index sensors
Chemical sensors
Polymer cavities
Thermo-optic coefficient

ABSTRACT

The present work relates to manufacturing of a simple interferometric optical fiber refractometer that features broad refractive index measuring range without ambiguity. The device consists of a cylindrical polymer cavity whose shape and dimensions are easily controllable. This in turn allows to control the performance of the refractometer. The signal processing is simple; it consists of calculating the amplitude and phase of the fast Fourier transform of the normalized interference spectra. In this manner, the refractive index value of the sample is obtained independently of the temperature. The refractometer can be used to measure the refractive index of liquids or viscous samples and can operate in a broad wavelength range. As an application, we demonstrate the measuring of the refractive index of gels at different temperatures from which the thermo-optic coefficient can be calculated.

1. Introduction

Refractometers are devices that measure the refractive index of a sample. They have been important in many industrial and scientific applications during centuries. Commercial refractometers measure the refractive index of a sample deposited on the lateral face of a prism of known refractive index. Such refractometers operate at the industry standard wavelength of 589 nm, but they can be modified to operate at infrared wavelengths [1,2]. The measuring range of prism-based refractometers is limited to indices that are smaller than that of the prism, which is typically around 1.5 or 1.7. Commercial refractometers are precise because they use several opto-mechanical components and have a system to keep the sample at constant temperature during the measurements.

Miniaturization and multiplexing of prim-based refractometers is complicated. Moreover, they cannot be used as refractive index sensors. Thus, they are not appropriate for refractometry in small spaces such as in microfluidics channels or in flowers *in vivo* [3–5]. For these applications, refractometers (index sensors) based on optical fibers are good candidates. The challenge in this case is to achieve devices that have not only miniature dimensions but that can measure indices in a broad measuring range, at least from 1.3 to 1.7; resolution comparable or higher to that of commercial refractometers, which is on the order of 10^{-4}, and ideally temperature independence. In addition, the fabrication of the refractometer must be highly reproducible and the cost of the device must be low. To achieve all these features, the optical fiber sensing community has proposed a myriad of alternatives.

Up to date, different techniques have been proposed to measure the refractive index of a sample with optical fibers. In one of them, the sample under test alters the guided light through direct interaction with the evanescent waves [6–11] or by means of thin layers [12–15]. Another alternative is to use tilted Bragg gratings [16–19]. Refractometers based on evanescent wave interactions or on tilted gratings require an interaction length of several millimeters and can measure indices in a narrow range, typically between 1.3 and 1.45. Moreover, they are highly sensitive to temperature. Another technique exploits the Fresnel reflection of an optical-fiber-sample interface, which depends on the refractive index of the fiber core and that of the sample [20–24]. This technique requires a sophisticated interrogation system to compensate fluctuations of the light source or bending losses in the optical fiber. However, its main drawback is the fact that two values of refractive index can give the same result. In refractive index sensing, this issue is called ambiguity.

Fabry-Perot interferometry (FPI) is another powerful technique to

* Corresponding author at: Department of Communications Engineering, University of the Basque Country UPV/EHU, Bilbao 48013, Spain.
E-mail address: agustinjoel.villatoro@ehu.eus (J. Villatoro).

https://doi.org/10.1016/j.optlastec.2021.106977
Received 29 October 2020; Received in revised form 19 December 2020; Accepted 27 January 2021
Available online 10 February 2021

measure refractive index of a sample and it has reached commercial level [25]. In this technique, a microscopic cavity is fabricated on the facet of an optical fiber. The sample under test can be placed inside the cavity [26–28] or outside of the same [29–33]. In either case, the interference pattern of the interferometer changes in proportion of the refractive index of the sample. Such changes can be quantified in different manners. A drawback of commercial FPI-based refractometers is their limitation to liquid samples only since viscous samples cannot be inserted easily in a microscopic cavity. The issues of other FPI-based refractive index sensors reported until now [26–33] include complex, hence, costly fabrication processes, in some cases limited measuring range, ambiguity, or temperature sensitivity.

Here, we report on a simple refractometer based on a FPI with cylinder polymer cavity that may overcome the aforementioned issues. Our device consists of a conventional single mode fiber (SMF) inserted in a standard ceramic ferrule. A cylindrical cavity with controllable dimensions is achieved between the SMF facet and the end of the ferrule. The cavity is filled with a UV-curable polymer whose refractive index is different than that of the SMF core. The interference pattern is controlled with proper dimensions of the cavity. By means of the amplitude and phase of the fast Fourier transform, a value that correlates unambiguously with the refractive index of the sample is obtained. The optical fiber refractometer reported here can measure indices of liquids and viscous fluids such as gels. To the best of our knowledge, the measuring range of our interferometric refractometer is one of the broadest reported until now. The resolution of our device is around 4×10^{-4}, which is sufficient for a variety of practical applications.

2. Device fabrication and working mechanism

The proposed refractometer is easy to fabricate and its interrogation is simple. A schematic representation of the device and its interrogation as well as a photograph of a fabricated device are shown in Fig. 1. The fabrication steps are the following. First, a cleaved or polished SMF is inserted in a ferrule that has an internal void with diameter approximately equal to that of the fiber. The latter reaches the end of the ferrule. To ensure this, an USB microscope (from Dino-Lite) was used. Then, a small amount of UV-curable polymer is deposited on the tip of the ferrule that is held fixed and in vertical position. After that, the fiber is moved slowly a distance d towards the interior of the ferrule. To do so, a motorized translation stage was used. In this manner, d, i.e., the cavity size of the interferometer can be controlled with micrometer or nanometer precision. Due to surface tension, the fiber withdraws the polymer as it moves, thus, a cavity of length d filled with polymer is formed at the end of the ferrule; see Fig. 1(a). Immediately after this, the polymer is cured with UV light.

All the steps mentioned above are easy to carry out and are reproducible. This is an important advantage over other FPIs with polymer cavities proposed in the literature in which the shape and dimensions of the cavity cannot be controlled [34–38].

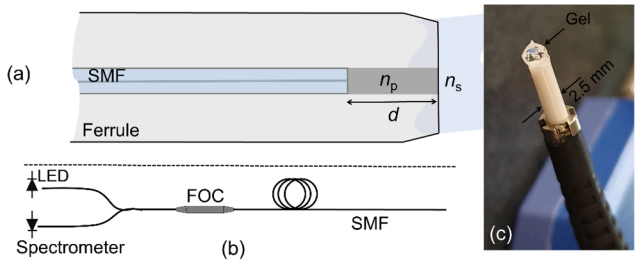

Fig. 1. (a) Diagram of the refractometer. SMF is single mode fiber, n_p and d are, respectively, the refractive index and length of the FPI cavity, n_s is the refractive index of the sample. (b) Scheme of the device interrogation. LED is the light source and FOC is fiber optic coupler or circulator. (c) Photograph of a fabricated sample with gel on top.

To fabricate our samples, we used a commercial polymer known as NOA81 (from Norland Optical Adhesives). The cavities were cured in 20 s. As recommended by the manufacturer, to improve the adhesion of the polymer to the fiber and the ferrule, the devices were cured at 60 °C during 12 h. To achieve a flat surface at the tip of the ferrule, it was polished during 10 s with a conventional fiber polisher. In this manner, the polymer protruding from the ferrule was removed. Note that two flat parallel interfaces were achieved; one formed between the fiber end face and the polymer, and the other between the polymer and the external environment.

To explain the working mechanism of our device, it is important to understand the beams that participate in the interference. As the fiber used to fabricate the device shown in Fig. 1(a) is single mode, two Gaussian beams participate in the interference. A beam is internally reflected from the SMF-polymer interface and the other beam is reflected from the polymer-sample interface. The amplitude coefficient from the fiber core-polymer interface can be denoted as $r_1 = (n_f - n_p)/(n_f + n_p)$, where n_f and n_p are, respectively, the refractive index of the SMF core and of the polymer. The amplitude coefficient from the polymer-sample interface is $r_2 = (n_p - n_s)/(n_p + n_s)$, where n_s is the index of the sample. It is important to point out that the values of r_1 and r_2 are independent of the polarization of the light. As the FPI cavity has no core, the Gaussian beam that reflects from the polymer-sample interface will return broader to the SMF due to diffraction.

As demonstrated by some of the present authors, the total reflected intensity of the device depicted in Fig. 1(a) is the superposition of two Gaussian beams. The intensity will be periodic in wavelength (λ) whatever the polarization of the incident light. The reflected intensity can be expressed as [37,38]:

$$I_r = r_1^2 + \eta^2 r_2^2 (1 - r_1)^4 + 2\eta r_1 r_2 (1 - r_1)^2 cos(2\phi) \quad (1)$$

In Eq. (1), $\phi = 2\pi d n_p/\lambda$ is the phase difference between the two Gaussian beams. In Eq. (1), the absorption of the NOA81 polymer was neglected, because, according to the manufacturer, the transmittance of such a polymer is approximately 95% from 500 to 1800 nm. The factor η is called the coupling coefficient or the overlapping coefficient of the two Gaussian beams which indicates how much light is coupled back to the fiber core. If the two reflecting surfaces are flat, such a factor can be expressed as [39]:

$$\eta = \left(\pi n_p w_0^2\right)^2 / \left[d^2\lambda^2 + \left(\pi n_p w_0^2\right)^2\right] \quad (2)$$

In Eq. (2), w_0 is the radius of the Gaussian beam at the output of the SMF, which is approximately a half of the mode field diameter (MFD) of the SMF. Depending on the manufacturer, the value of MFD at 1500 nm is between 9.5 and 10.5 μm.

Note from Eq. (2) that η is independent of n_s (the refractive index of the sample). On the other hand, the type of SMF, the material of the cavity, i.e., n_p, and the light source (or λ) can be chosen to fabricate and interrogate the refractometer. Thus, the critical parameter to control η, hence I_r, and consequently, the performance of the refractometer is the size of the cavity or d. As it was mentioned above, d can be controlled with micrometer, and even with nanometer, precision with a computer-controlled translation stage. Another important factor is the flatness of the interfaces from which the Gaussian beams reflect. In our case, this is not an issue as we cleave or polish the two reflecting surfaces mentioned above. The cleaving or polishing angle that can be achieved with conventional fiber cleavers or polishers is approximately 0.2°, and even less. Thus, a more accurate calculation of the coupling factor η can be carried out with Eqs. (A7) and (A8) of Ref. [40].

3. Results and discussion

In Fig. 2, we show the evolution of η for different values of d. For the calculations, we assumed that $w_0 = 5.0$ μm, which is an average value at $\lambda = 1550$ nm in conventional SMFs. In the figure, we show the values of η

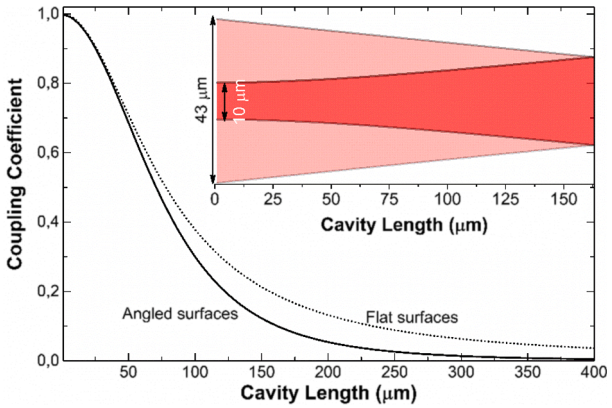

Fig. 2. Value of the coupling coefficient η as a function of the cavity length considering flat surfaces (dotted line) and ones with a angle of 0.2° (solid line). The inset shows the diffraction of a Gaussian beam, at λ = 1550 nm, when it leaves (dark red) and returns (light red) to the SMF.

when the interfaces are perfectly flat and when they have an angle of 0.2°. The value of the refractive index of the NOA81 polymer was calculated with the following equation provided by the manufacturer: $n_p = A + B/\lambda^2 + C/\lambda^4$, with $A = 1.5375$, $B = 8290.45$, and $C = -2.11046 \times 10^8$. The inset of Fig. 2 shows the propagation (at 1550 nm) of a Gaussian beam when it leaves an SMF, travels a distance $d = 163$ μm (dark red), and returns (light red) to the SMF after being reflected from a flat surface. The results shown in Fig. 2 suggest that d allows controlling the coupling coefficient η.

In Fig. 3, we show the theoretical reflection spectra of some FPIs with different lengths of the cavity that are indicated in the figure. In all cases, the reflection spectra were calculated with Eqs. (1) and (2) in which it was assumed that $n_s = 1$. It can be noted that the visibility of the interference patterns increases as d is longer. Visibility is defined as the difference over the sum of the maximum and minimum of the interference pattern. With the fabrication technique here described, the cavity size can be controlled with high precision; hence, the visibility of the interference patterns in our devices can be tailored. We will see that high visibility when the external medium is air is important to avoid ambiguity in the refractive index measurements.

3.1. Effect of temperature

The effect of temperature on our FPIs was studied first. To do so, a device fabricated with NOA81 polymer with $d = 125$ μm was placed in a temperature chamber. The device was exposed to temperatures between

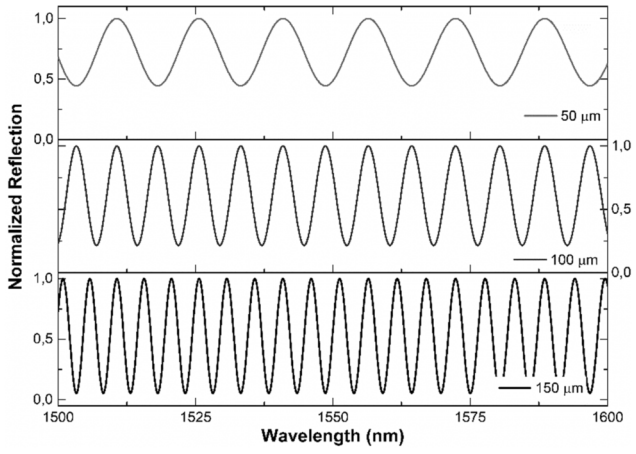

Fig. 3. Calculated reflection spectra of FPIs for three different values of d which are indicated in the graphs.

−10 and 45 °C. For this experiment, the external medium was air. Some of the observed spectra are shown in Fig. 4(a). As expected, the interference patterns shifted as the polymer that fills the cavity is temperature sensitive. The fast Fourier transform (FFT) of the spectra observed at different temperatures is shown in Fig. 4(b). From Fig. 4(b), it can be noted that the amplitude of the FFT (denoted as A_F) changed around 2.5% in the temperature range between 5 and 45 °C. At temperatures below 0 °C the changes are more prominent, however, refractometers are not designed to measure the index of samples at such temperatures as liquids may freeze. In the 20–25 °C range, A_F changes 3.1×10^{-4}.

It is important to discuss in more detail the behavior of our interferometers when they are exposed to different temperatures. To do so the optical properties of the NOA81 polymer must be taken into account. According to the manufacturer, such a polymer has a thermal expansion coefficient (TEC) at room temperature of 220×10^{-6} °C^{-1}. This means that a cavity of 125 μm will increase or decrease less than 1 μm if the temperature gradient is 30 °C. The thermo-optic coefficient (TOC) of the aforementioned polymer is -1.87×10^{-4} °C^{-1}. This means that a temperature gradient of 35 °C will change the refractive index of the polymer by 6.545×10^{-3}. The changes in d or in n_p give rise to shifts in the interference pattern but, according to the results shown in Fig. 4(b), the amplitude of the FFT does not change drastically.

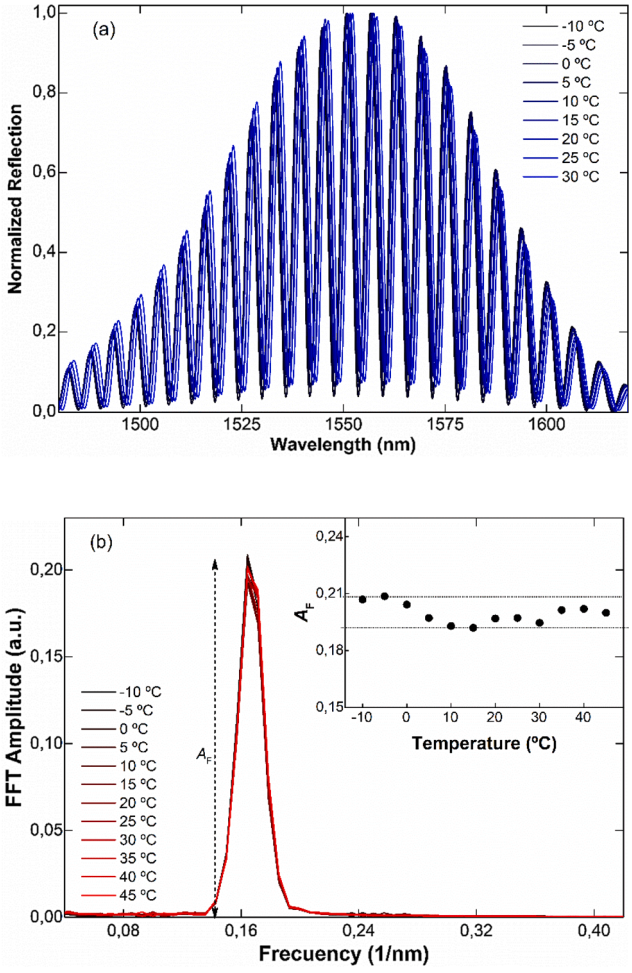

Fig. 4. (a) Experimental reflection spectra at different temperatures observed with a device in which $n_p = 1.5409$ and $d = 125$ μm. In all cases, the external medium was air. (b) FFT of the spectra shown in (a). The inset plot in shows the height of the FFT at different temperatures.

3.2. Refractive index measurements

To measure n_s, i.e. the refractive index of a sample, the following measuring procedure was implemented. First, it is important to fabricate a FPI with high visibility when the external medium is air. Second, the FFT of the normalized spectra are calculated of each value of n_s. From this calculation we obtain the amplitude and phase of the FFT, denoted here as A_F and ϕ_F, respectively. We will see that the value of A_F depends on n_s. In fact, some research groups have reported FPI-based refractive index sensors in which A_F is correlated with n_s, see for example [38,41]. The value of $\cos(\phi_F)$ -or $\sin(\phi_F)$- has the same sign for all values of n_s that are smaller than n_p and opposite sign for all values of n_s bigger than n_p due to phase changes as demonstrated in [29,41,42]. Thus, by normalizing the value of $\cos(\phi_F)$, to take into account exclusively its sign, it is possible to determine n_s without ambiguity if we calculate the following value:

$$S = \pm A_F \times cos(\phi_F)/|cos(\phi_F)|. \quad (3)$$

The sign in Eq. (3) can be chosen. In our case, S was considered to be positive when $n_s = 1$. In Fig. 5, we show the theoretical value of S as a function of n_s for three values of the coupling coefficient η, such values can be obtained with FPI with cavities with d between 50 and 150 μm. To obtain the results shown in Fig. 5, the cavity of the FPIs was considered to be made of a polymer with $n_p = 1.5409$. The wavelength was considered to be in the 1500–1600 nm range. The values of A_F and ϕ_F, and therefore, the value of S, were calculated from the FFT of the normalized reflection spectra for each value of n_s. The spectra were calculated with the expressions given in Eqs. (1) and (2). It can be noted that with a FPI where the coupling factor η is 0.2 it is possible to measure indices over a broad range without ambiguity. According to the results shown in Fig. 2 such coupling factor can be achieved with cavity with d in the 125–160 μm range.

To demonstrate the concepts outlined above, we fabricated a FPI with a commercial polymer (NOA81) whose n_p is 1.5409 at 1550 nm. The size of the cavity was 125 μm for the reasons explained above. The interference patterns were collected when the device was in air or in contact with calibrated refractive index liquids. In our case, we used brand new calibrated oils (from Cargille Labs). All the spectra were collected and normalized when the FPI and the oils were at 25 °C. The value of the indices of the oils at 1550 nm were calculated with the Cauchy equation for each oil provided by the manufacturer.

The measurements were carried out as follows. The reflection spectrum of the refractometer when it was in contact with each calibrated index was taken and normalized. In Fig. 6(a), we show the spectra observed at different indices. The values given in the figure are the indices of Cargille oils at 1550 nm. Between consecutive measurements, the surface of the polymer at the end of the ferrule was cleaned and dried. The normalization is important to eliminate the effect of fluctuations of the optical source or losses caused by mechanical connectors in the calculation of the FFT.

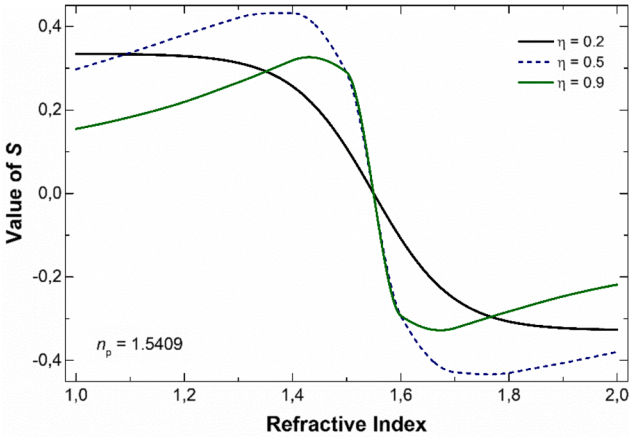

Fig. 5. Calculated value of S as a function of the refractive index (n_s). For the calculations, the values of η shown in the plot were considered. In all cases, n_p was considered to be 1.5409.

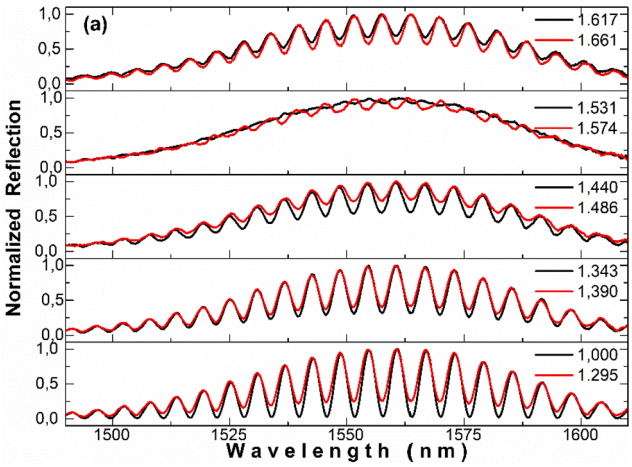

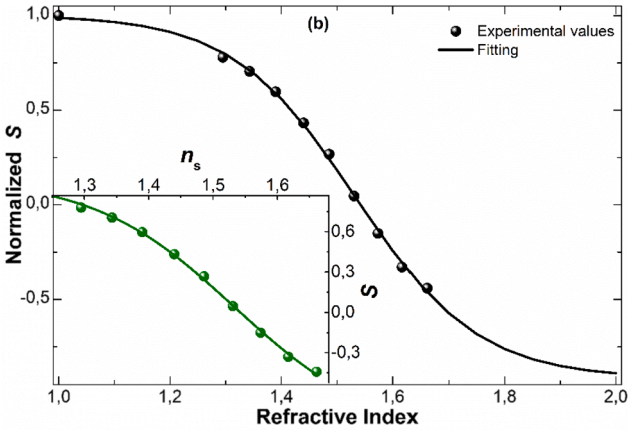

Fig. 6. (a). Reflection spectra observed when the interferometer was in contact with the indices indicated in the figure. (b) Normalized value of S as a function of refractive index. The solid dots are experimental points and the continuous line is the fitting to the data. The parameters of the FPI were: $n_p = 1.5409$ and $d = 125$ μm. The inset graph is a closed up of the region where n_s was calibrated.

In Fig. 6(b), we show the experimental values of S as a function of n_s. The values of S were calculated with the amplitude and phase of the FFT obtained from the normalized spectra shown in Fig. 6(a). For simplicity, S was considered to be 1 when n_s was 1. The inset graph shows only the values of S obtained with calibrated refractive index oils. In the graphs, the solid dots are experimental points and the solid lines are a fitting to the experimental data that was extrapolated to $n_s = 2$. It can be noted from the figure that the fitting to the experimental data leads to a curve of sigmoidal shape.

From the fitting of the experimental data, the value of ns can be calculated with the following expression:

$$n_s = n_0 - \left(\frac{1}{p}\right)\log\left(\frac{S_2 - S_1}{S - S_1} - 1\right) \quad (4)$$

In Eq. (4), S_2, S_1, n_0, and p are fitting values that can be calculated easily for each sensor. The slope of the fitting curve is p and n_0 is the point where S is zero. Therefore, according to Eqs. (3) and (4), a measurement of S will lead to a unique value of n_s no matter the value of it in the range between 1 and 2. To the best of the authors' knowledge, the measuring range of the fiber refractometer discussed here is the broadest

one reported until now.

The capability of our device to measure refractive indices of viscous samples was investigated. To do so, the device with $d = 125$ μm described above was immersed in a commercial index matching gel (G608N3 purchased from Thorlabs) whose index and TOC were, respectively, 1.4382 (at 1550 nm) and $-3.5 \times 10^{-4}\,^{\circ}\mathrm{C}^{-1}$. The device and the gel were exposed to temperatures between −10 and 35 °C in a temperature chamber. Some of the observed spectra are shown in Fig. 7 (a).

In Fig. 7(b), we show the FFT amplitude as a function of frequency at different temperatures. Such plots were calculated from the spectra shown in Fig. 7(a). The alteration of A_F is attributed to refractive index changes of the gel, which are caused by the effect of temperature. Different values of refractive indices of the gel give rise to different values of A_F. Note from Fig. 7(b) that the value of A_F increases with temperature. According to the calibration curve shown in Fig. 6, this means that the gel refractive index diminishes with temperature, which agrees well with the fact that the TOC of the gel is negative.

From the calibration procedure discussed above and the values of A_F from Fig. 7(b), we calculated n_s of the gel at different temperatures. The results are shown in Fig. 8. In such a graph, the squares represent the index of the gel measured with our refractometer and the continuous solid line is the index of the gel as a function of temperature that was calculated with the data (refractive index and TOC) provided by the gel manufacturer. From the experimental data shown in Fig. 8, the index of the gel as a function of temperature was found to be $n_s = 1.4468 - 3.4011 \times 10^{-4}T$. In this expression, T is temperature in degree Celsius.

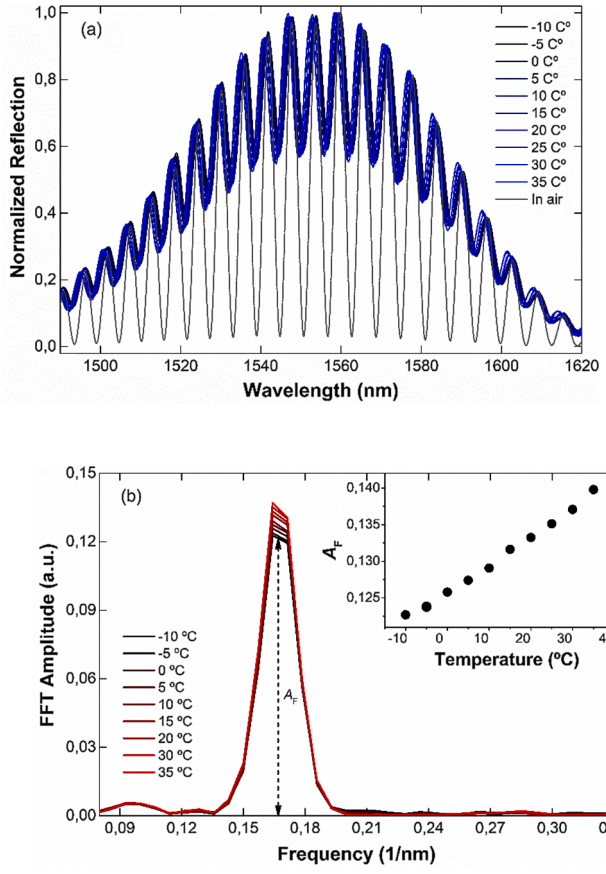

Fig. 7. (a) Reflection spectra of a FPI fabricated with $n_p = 1.5409$ and $d = 125$ μm at different temperatures when the external medium was a gel ($n_s = 1.4382$) with high thermo-optic coefficient. The spectrum when the external medium was air is included for comparison. (b) FFT amplitude as a function of frequency observed at different temperatures. Such values were calculated from the plots shown in Fig. 7(a).

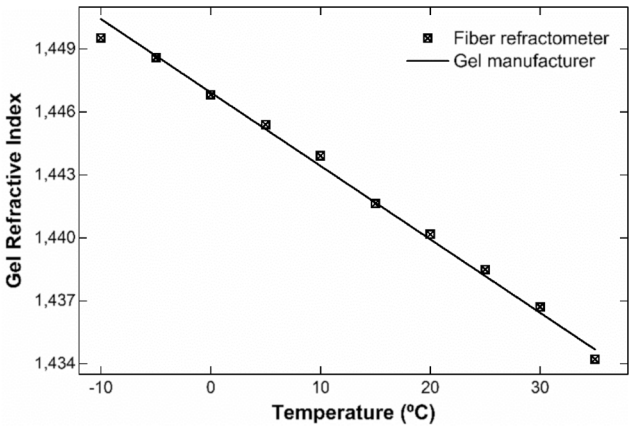

Fig. 8. Refractive index of a commercial gel with high thermo-optic coefficient as a function of temperature. The squares are values measured with the FPI described in Fig. 7 and the solid line represents the values provided by the gel manufacturer.

This means that the TOC of the aforementioned gel measured with our device was -3.4011×10^{-4}. The difference with the value given by the manufacturer is 9.89×10^{-6}. The results shown in Fig. 8 suggest that our device without a reference temperature sensosr can be used to calculate, with good approximation, the TOC of different gels or liquids. For this application, our device is simpler than other fiber optic sensors reported so far, see for example [43–45].

4. Conclusions

In this work, we have reported on a compact fiber optic interferometer that comprises a conventional mono mode fiber inside a ferrule. At the end of the latter, a cylindrical polymer cavity is made. The dimensions of the cavity can be controlled with high precision with a motorized translation stage. This fabrication process ensures reproducibility.

The interferometer proposed here can be used as a refractometer for liquid and viscous samples. For this application, it was demonstrated that a cavity with properly selected dimensions in combination with an adequate signal processing allows the measuring of refractive indices over a broad range, at least from 1.3 to 1.7, without ambiguity. Moreover, the signal processing discussed here allows the measuring of refractive index without a reference temperature sensor. Under these conditions, the errors in the refractive measurements can be on the order of 10^{-4} if the temperature gradient is not so high. Therefore, the refractometers proposed here can be used in laboratory environments without temperature compensation. The attributes of our refractometer combined with its small dimensions and its multiplexing capability, which is an attribute of most optical fiber sensors, make it attractive for a number of practical applications, particularly for those in small or remote spaces.

We believe that the interferometers reported here can be used as sensors as well. For such applications, the cavity of the interferometer must be coated with polymers, resins or any other material that is sensitive to a chemical or biological parameter. Therefore, the concepts and approaches reported here can lead to the development of a variety of devices.

CRediT authorship contribution statement

J.A. Flores-Bravo: Conceptualization, Methodology, Formal analysis. **M.A. Illarramendi:** Investigation, Formal analysis, Writing - review & editing. **Joseba Zubia:** Resources, Formal analysis, Funding acquisition. **Joel Villatoro:** Conceptualization, Visualization, Formal analysis, Supervision, Writing - review & editing.

Declaration of Competing Interest

The authors declare that they have no known competing financial interests or personal relationships that could have appeared to influence the work reported in this paper.

Acknowledgments

The authors acknowledge funding support from the Fondo Europeo de Desarrollo Regional (FEDER) and the Ministerio de Economia y Competitividad (Spain) under projects PGC2018-101997-B-I00 and RTI2018-094669-B-C31, and also from the Departamento de Educación del Gobierno Vasco, grants No. IT933-16 and Elkartek KK2019-00101.

References

[1] J. Rheims, J. Köser, T. Wriedt, Refractive-index measurements in the near-IR using an Abbe refractometer, Measure. Sci. Technol. 8 (1997) 601–605.
[2] J.E. Saunders, C. Sanders, H. Chen, H.-P. Loock, Refractive indices of common solvents and solutions at 1550 nm, Appl. Opt. 55 (2016) 947–953.
[3] L. Lei, H. Li, J. Shi, Y. Chen, Microfluidic refractometer with integrated optical fibers and end-facet transmission gratings, Rev. Sci. Instrum. 81 (2010) 023103.
[4] S.Y. Yoon, S. Yang, Microfluidic refractometer with micro-image defocusing, Lab Chip 11 (2011) 851–855.
[5] G. Aronne, P. Malara, Fiber-optic refractometer for in vivo sugar concentration measurements of low-nectar-producing flowers, New Phytol. 224 (2019) 987–993.
[6] Q. Wang, G. Farrell, All-fiber multimode-interference-based refractometer sensor: proposal and design, Opt. Lett. 31 (2006) 317–319.
[7] R. Jha, J. Villatoro, G. Badenes, V. Pruneri, Refractometry based on a photonic crystal fiber interferometer, Opt. Lett. 34 (2009) 617–619.
[8] H. Gong, C.C. Chan, Y.F. Zhang, W.C. Wong, X. Dong, Miniature refractometer based on modal interference in a hollow-core photonic crystal fiber with collapsed splicing, J. Biomed. Opt. 16 (2011) 017004.
[9] Q. Wu, Y. Semenova, P. Wang, G. Farrell, High sensitivity SMS fiber structure based refractometer–analysis and experiment, Opt. Express 19 (2011) 7937–7944.
[10] J. Wu, Y. Miao, B. Song, K. Zhang, W. Lin, H. Zhang, B. Liu, J. Yao, Temperature-insensitive optical fiber refractometer based on multimode interference in two cascaded no-core square fibers, Appl. Opt. 53 (2014) 5037–5041.
[11] P. Wang, S. Zhang, R. Wang, G. Farrell, M. Zhang, T. Geng, E. Lewis, K. Tian, Temperature-insensitive refractometer based on an RI-modulated singlemode-multimode-singlemode fibre structure, Opt. Express 27 (2019) 13754–13764.
[12] M. Iga, A. Seki, K. Watanabe, Hetero-core structured fiber optic surface plasmon resonance sensor with silver film, Sens. Actuators, B 101 (2004) 368–372.
[13] S.M. Tripathi, A. Kumar, E. Marin, J. Meunier, Side-polished optical fiber grating-based refractive index sensors utilizing the pure surface plasmon polariton, J. Lightwave Technol. 26 (2008) 1980–1985.
[14] J.S. Velázquez-González, D. Monzón-Hernández, D. Moreno-Hernández, F. Martínez-Piñón, I. Hernández-Romano, Simultaneous measurement of refractive index and temperature using a SPR-based fiber optic sensor, Sens. Actuators, B 242 (2017) 912–920.
[15] A. Ozcariz, D.A. Piña-Azamar, C.R. Zamarreño, R. Dominguez, F.J. Arregui, Aluminum doped zinc oxide (AZO) coated optical fiber LMR refractometers—an experimental demonstration, Sens. Actuators, B 281 (2019) 698–704.
[16] C.F. Chan, C. Chen, A. Jafari, A. Laronche, D.J. Thomson, J. Albert, Optical fiber refractometer using narrowband cladding-mode resonance shifts, Appl. Opt. 46 (2007) 1142–1149.
[17] B. Jiang, K. Zhou, C. Wang, Y. Zhao, J. Zhao, L. Zhang, Temperature-calibrated high-precision refractometer using a tilted fiber Bragg grating, Opt Express 25 (2017) 25910–25918.
[18] W. Zhou, Y. Zhou, J. Albert, A true fiber optic refractometer, Laser Photonics Rev. 11 (2017) 1600157.
[19] Z. Zhang, T. Guo, B.-O. Guan, Reflective fiber-optic refractometer using broadband cladding mode coupling mediated by a tilted fiber Bragg grating and an in-fiber mirror, J. Lightwave Technol. 37 (2019) 2815–2819.
[20] C.-B. Kim, C.B. Su, Measurement of the refractive index of liquids at 1.3 and 1.5 micron using a fibre optic Fresnel ratio meter, Meas. Sci. Technol. 15 (2004) 1683–1686.
[21] H. Su, X.G. Huang, Fresnel-reflection-based fiber sensor for on-line measurement of solute concentration in solutions, Sens. Actuators, B 126 (2007) 579–582.
[22] J.R. Zhao, X.G. Huang, J.H. Chen, A Fresnel-reflection-based fiber sensor for simultaneous measurement of liquid concentration and temperature, J. Appl. Phys. 106 (2009) 083103.
[23] A. Basgumus, F.E. Durak, A. Altuncu, G. Yılmaz, A universal and stable all-fiber refractive index sensor system, IEEE Photonics Technol. Lett. 28 (2016) 171–174.
[24] R. Martinez-Manuel, M.D.R. Bautista-Morales, D. Lopez-Cortes, C.A. Pineda-Arellano, M.G. Shlyagin, O. Esteban, Multi-point fiber refractometer using Fresnel reflection and a coherent optical frequency-domain multiplexing technique, Appl. Opt. 58 (2019) 684–689.
[25] É. Pinet, Fabry-Pérot fiber-optic sensors for physical parameters measurement in challenging conditions, Journal of Sensors 2009 (2009).
[26] C.J. Alberts, S.d. Man, J.W. Berenschot, V.J. Gadgil, M.C. Elwenspoek, D. Iannuzzi, Fiber-top refractometer, Measure. Sci. Technol., 20 (2009) 034005.
[27] E. Cibula, D. Donlagic, In-line Fabry-Perot refractive index sensor, IEEE Photonics Technol. Lett. 23 (2011) 1609–1611.
[28] C.-L. Lee, Y. Lu, C.-H. Chen, C.-T. Ma, Microhole-pair hollow core fiber Fabry-Perot interferometer micromachining by a femtosecond laser, Sens. Actuators, A 302 (2020) 111798.
[29] Z.L. Ran, Y.J. Rao, W.J. Liu, X. Liao, K.S. Chiang, Laser-micromachined Fabry-Perot optical fiber tip sensor for high-resolution temperature-independent measurement of refractive index, Opt. Express 16 (2008) 2252–2263.
[30] L. Mosquera, D. Saez-Rodriguez, J.L. Cruz, M.V. Andres, In-fiber Fabry-Perot refractometer assisted by a long-period grating, Opt Lett 35 (2010) 613–615.
[31] P. Chen, X. Shu, H. Cao, K. Sugden, High-sensitivity and large-dynamic-range refractive index sensors employing weak composite Fabry-Perot cavities, Opt. Lett. 42 (2017) 3145–3148.
[32] Y. Ouyang, X. Xu, Y. Zhao, A. Zhou, L. Yuan, Temperature compensated refractometer based on parallel fiber Fabry-Pérot interferometers, IEEE Photonics Technol. Lett. 30 (2018) 1262–1265.
[33] O. Rodríguez-Quiroz, C.E. Domínguez-Flores, D. Monzón-Hernández, E. Morales-Narváez, V.P. Minkovich, D. López-Cortés, Unambiguous refractive-index measurement in a wide dynamic-range using a hybrid fiber Fabry-Perot interferometer assisted by a fiber Bragg grating, Optics Laser Technol. 128 (2020) 106236.
[34] O. Frazao, P. Caldas, J.L. Santos, P.V. Marques, C. Turck, D.J. Lougnot, O. Soppera, Fabry-Perot refractometer based on an end-of-fiber polymer tip, Opt Lett 34 (2009) 2474–2476.
[35] V. Melissinaki, M. Farsari, S. Pissadakis, A fiber-endface, Fabry-Perot vapor microsensor fabricated by multiphoton polymerization, IEEE J. Sel. Top. Quantum Electron. 21 (2014) 344–353.
[36] X. Tan, Y. Geng, X. Li, Y. Deng, Z. Yin, R. Gao, UV-curable polymer microhemisphere-based fiber-optic Fabry-Perot interferometer for simultaneous measurement of refractive index and temperature, IEEE Photonics J. 6 (2014) 1–8.
[37] O. Arrizabalaga, G. Durana, J. Zubia, J. Villatoro, Accurate microthermometer based on off center polymer caps onto optical fiber tips, Sens. Actuators, B 272 (2018) 612–617.
[38] O. Arrizabalaga, J. Zubia, J. Villatoro, Microrefractometer based on off-center polymer caps bonded onto optical fiber tips, J. Lightwave Technol. 36 (2018) 3573–3579.
[39] N. Ushakov, L. Liokumovich, Resolution limits of extrinsic Fabry-Perot interferometric displacement sensors utilizing wavelength scanning interrogation, Appl. Opt. 53 (2014) 5092–5099.
[40] Y. St-Amant, D. Gariépy, D. Rancourt, Intrinsic properties of the optical coupling between axisymmetric Gaussian beams, Appl. Opt. 43 (2004) 5691–5704.
[41] O. Rodríguez-Quiroz, C.E. Domínguez-Flores, D. Monzón-Hernández, C. Moreno-Hernández, Hybrid fiber Fabry-Perot interferometer with improved refractometric response, J. Lightwave Technol. 37 (2019) 4268–4274.
[42] M.G. Shlyagin, R. Martínez Manuel, Ó. Esteban, Optical-fiber self-referred refractometer based on Fresnel reflection at the fiber tip, Sens. Actuators, B 178 (2013) 263–269.
[43] Y.H. Kim, S.J. Park, S.-W. Jeon, S. Ju, C.-S. Park, W.-T. Han, B.H. Lee, Thermo-optic coefficient measurement of liquids based on simultaneous temperature and refractive index sensing capability of a two-mode fiber interferometric probe, Opt. Express 20 (2012) 23744–23754.
[44] Y. Chen, L. Fang, D. Yi, X. Li, X. Hong, Thermo-optic property measurement using surface plasmon resonance-based fiber optic sensor, IEEE Sens. J. 20 (2020) 11357–11363.
[45] V. Ruiz-Perez, P. Velasco-Bolom, D. May-Arrioja, J. Guzman-Sepulveda, Measuring the thermo-optic coefficient of liquids with athermal multimode interference devi ces, IEEE Sens. J. (2020).